Fracturing due to fluid intrusion into viscoelastic materials

T. Hirata
Institute of Applied Physics, University of Tsukuba, Tsukuba, Ibaraki 305, Japan
(Received 28 May 1996; revised manuscript received 7 October 1997)

Fluid intrusion into viscoelastic materials is studied by changing the viscoelastic property of a model material (agar gel) from a viscous fluid to an elastic solid. Viscous fingering is observed in the agar gel with a low concentration of agar and single plane cracking are observed in the agar gel with a high concentration of agar in our experiments. At the middle range of agar concentration, a new kind of pattern growth called ''viscoelastic fracturing'' is observed due to two competitive mechanism (viscous flow and fracture). A phase diagram for pattern formation is obtained as a function of the fluid injection pressure and the concentration of agar. Fractal dimensions for these patterns are calculated. The fractal dimension for the viscoelastic fracturing patterns ranges from 1.85 to 1.95, which is considerably different from the value $D=1.68$ for diffusion-limited aggregation. [S1063-651X(98)13302-0]

PACS number(s): 47.90.+a, 46.30.Nz, 83.90.+s

I. INTRODUCTION

An intrusion of a fluid into a fluid or a solid shows various interfacial patterns. When a lower viscosity fluid is injected into a Hele-Shaw cell filled with a higher viscosity fluid, viscous fingering is observed [1–4]. Under certain conditions, a viscous finger shows a fractal pattern formation [5,6], which has been studied extensively as a prototype of fractal growth [7,8]. The fractal pattern formation is observed in a wide range of interdisciplinary fields: some examples are fluid flow in porous media [9], dielectric breakdown [10], dendritic solidification [11–13], colloidal particle aggregation [14], and electrodeposition [15,16]. In the case of a fluid intrusion into a brittle solid, crack propagation occurs by hydraulic fracturing. Single plane cracking is often seen in brittle fracture due to fluid intrusion; for instance, a dike which has a sheetlike form, such as Spanish Peaks [17], is an example of single plane cracking generated by magma intrusion into crust [18,19]. Hydraulic fracturing is not only an interesting phenomenon, but also has many important geophysical applications. These applications include making in situ stress measurements [20], creating conduits of hot water in a geothermal energy extraction (known as Hot Dry Rock Project [21,22]), and similar applications in the oil industries. These interfacial pattern growths are one of most exciting topics, not only in physics but also in engineering and other fields.

Recently fracture phenomena, including hydraulic fracturing [23,24], have attracted the interest of physicists, and have been investigated intensively [25–31]. These studies are mainly concerned with a brittle fracture. However, brittle fracture is, in a sense, an extreme case of hydraulic fracturing. Many materials in nature have viscoelastic properties: composite materials, polymers, etc. Although a rock is a typical brittle material, an earthquake is an example of brittle fracture of rock, and also behaves as a viscous fluid depending on the strain rate. At a very low strain rate, rock can be treated as a viscous fluid, e.g., mountain formation or mantle convection.

The intrusion of a fluid into a viscoelastic material gives rise to many interesting phenomena. In the case of viscoelastic materials, there are two ways of releasing stresses: viscous flow and fracture. Recently, fluid injection experiments were performed in which a Hele-Shaw cell was filled with colloidal fluids [32]. In these experiments, clay solutions were used as viscoelastic materials. Viscoelastic materials are primarily divided into two categories, according to their flow behavior: fluid or solid [33]. The Maxwell fluid and Kelvin solid are typical examples. The Maxwell material can be explained by a spring and dashpot in a series that behaves like a fluid on a long time scale. The Kelvin solid can be described by a combination of spring and dashpot in parallel, which behaves like a solid on a long time scale. This is the reason why they are called a Maxwell fluid and a Kelvin solid. Previous experiments emphasized the viscoelastic fluids rather than viscoelastic solids. Our experiment focuses more on the fracturing process in viscoelastic materials, by choosing an agar gel that shows an elastic fracture as a model of viscoelastic materials.

II. EXPERIMENTS

A. Experimental setup

Our experiments were carried out under a constant injection pressure of air in a radial Hele-Shaw cell (Pyrex glass plate and acrylic acid resin vessel spaced 2 mm apart: $300\times300\times2\ \mathrm{mm}^3$) filled with viscoelastic materials. Air (viscosity $\sim1.82\times10^{-5}$ Pa s) was injected into the Hele-Shaw cell through a 2.5-mm hole at the center of the upper Pyrex glass plate. The plastic tube with inner radius 2.5 mm and outer radius 3.0 mm, in diameter, was attached to the center of the Pyrex glass. The maximum air supply ability of the experiment system at the injection pressure of 2.0 kPa was about $1.0\times10^2\ \mathrm{cm}^3/\mathrm{s}$, which corresponds closely to the value estimated by assuming a Poiseuille flow ($1.05\times10^2\ \mathrm{cm}^3/\mathrm{s}$) in the plastic tube. The injection pressure of air is measured during the experiments. Within a measurement accuracy of the pressure monitor system of ±0.01 kPa, no fluctuation of injection pressure is observed during pattern growth. The Hi-8 CCD video camera was used to measure the dynamical pattern growth. A video camera can record images at a rate of 30 frames a second. Therefore, the

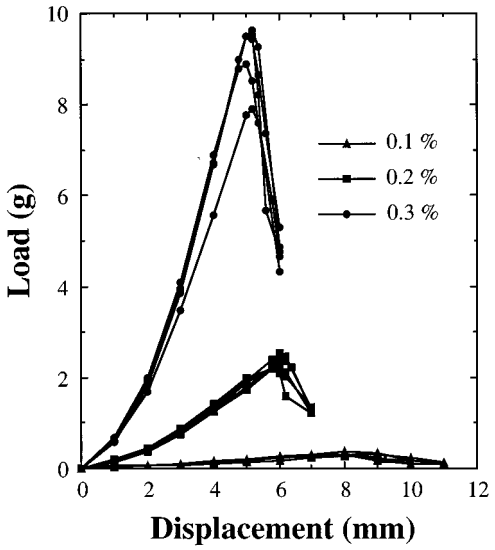

FIG. 1. Relation between load and displacement for agar gels of 0.1-, 0.2-, and 0.3-wt % agar concentration. The indentation experiments using the rod with the hemispherical head of 10 mm in diameter were carried out five times for each agar concentration. The rod was moved downward upon the 300-cc beaker filled with 200-cc agar gels at a speed of 0.2 mm/s.

dynamical interfacial growth of patterns can be monitored with an accuracy of $\frac{1}{30}$ of a second.

B. Fracture and viscoelastic properties of agar gels

An agar gel made from an extra pure reagent agar powder by Nacalai Tesque, Inc. [the gel strength defined by the Japan Agricultural Standard (JAS) was 600–700 g/cm^2] was used as a model material of a viscoelastic body [34,35]. The viscoelastic properties of agar gels are easily controlled by changing the concentration of agar from a viscous fluid to an elasticity body. An agar solution becomes a gel between 0.1 and 0.4 wt %. Because viscous flow and tensile fracture play important roles in air intrusion into a viscoelastic material, one needs to know both the properties of a viscous flow and a fracture of a model material.

Figure 1 shows the displacement vs load relations of agar gels with concentrations of 0.1-, 0.2-, and 0.3-wt % agar. Although the gel strength of a 1.5-wt % agar gel defined by JAS that is similar to those defined by Marine Colloids or Meer Corp. is widely used in the commercial evaluation of agar quality [34], its value is not useful for our purpose because it is a rough estimation of the gel strength around the agar concentration of 1.5 wt %. Since the agar gel is too weak to carry out a usual strength test such as a tensile test, the following experiment was performed to determine a relative strength as a function of the agar concentration: A glass rod 10 mm in diameter with a hemispherical head was inserted in the beaker filled with agar until the occurrence of a tensile fracture at a moving speed of 0.2 mm/s. Here the displacement is the amount of insertion of the glass rod measured after touching the surface of the agar gel. Although the fracture strength depends on strain rates, we can define it as the fracture strength where the load decreases abruptly. The fracture strength increases with an increasing concentration of agar. The displacement where the breakdown occurs decreases with an increasing concentration of agar. We carried out fracture experiments five times for each agar concentration to obtain load-displacement curves. The data show a good reproducibility between different agar gel samples. The ratio of relative strength of agar gels with 0.1-, 0.2-, and 0.3-wt % agar concentrations are 0.14:1.0:3.9 (normalized by the strength of 0.2-wt % agar gel). The average displacement of the glass rod insertion at which tensile fractures occur are 8.2, 6.0, and 5.1 mm, respectively. Although this should be considered a rough estimation, the stress field of the agar gel can be estimated according to Hertz's classic elastic contact theory. The estimation of the maximum stress of 0.3-wt % agar gel at the fracture point is 1.7 kPa, which can be regarded as a tensile strength of the 0.3-wt % agar gel. The properties of the fracture strength are summarized in Table I.

TABLE I. Relative strength of agar gels.

Concentration of agar (wt %)	Load (g)	Relative strength	Displacement (mm)
0.1	0.31 (s.d. 0.04)	0.14	8.2 (s.d. 0.44)
0.2	2.31 (s.d. 0.15)	1	6.0 (s.d. 0.14)
0.3	9.10 (s.d. 0.72)	3.9	5.1 (s.d. 0.11)

The viscosity of agar gels of concentration of 0.05–0.15-wt % agar were measured by the rotation cylinder type viscosity meter with accuracy of $\pm 10\%$. A pure viscosity cannot be defined in a viscoelastic material such as the agar gel. However, agar gels with lower concentration of agar (0.05–0.15 wt %) wer considered to be a viscous fluid, and the viscosity was measured here. The viscosity of agar gel increases with an increasing concentration of agar, as shown in Fig. 2. The viscosity increases dramatically between 0.10 wt % and 0.15%. At concentrations of agar higher than 0.20 wt %, the assumption that the agar gel behaves like a viscous fluid are invalid. Instead of viscosity measurements, the stress relaxation experiments were performed for the agar gels with concentrations of 0.2- and 0.3-wt % agar to deter-

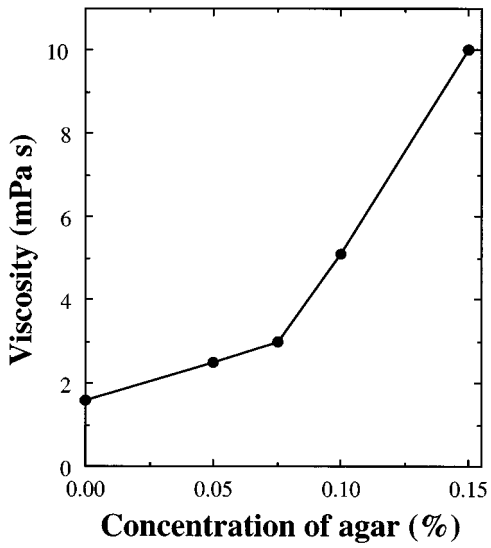

FIG. 2. The viscosity is plotted against the concentration of agar.

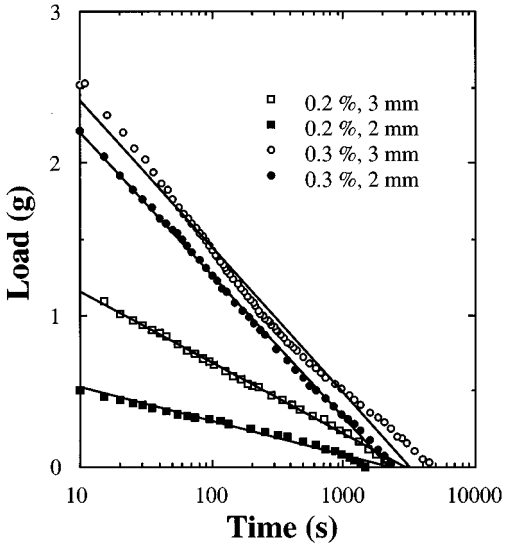

FIG. 3. Dependence of the load on the time for the agar gels with the agar concentration of 0.2 and 0.3 wt %. The load obtained by both 2- and 3-mm rod insertions is plotted against the time. The rod with the hemispherical head of 10 mm in diameter was also used for the relaxation experiment. The rod was moved downward up to 2- or 3-mm insertions at a speed of 0.2 mm/s, and then the rod was held at the position.

mine their flow property. The glass rod was stopped after 2- or 3-mm insertion at the moving speed of 0.2 mm/s, then a temporal change of load was measured. The load of 0.2- and 0.3-wt % agar gels are plotted against the time on semilogarithmic scale in Fig. 3. Both data sets corresponding to a 2- and 3-mm insertion of the glass rod are shown in Fig. 3. If the agar gel is a complete elastic body, no relaxation of load with time is observed. However, in both experiments of 0.2- and 0.3-wt % agar gels, the load relaxation phenomena were observed. In order to compare the degree of flow between 0.2- and 0.3-wt % agar, we calculated the time needed to relax the load from 1.0 to 0.0 g. The time needed to relax from 1.0 to 0.0 g for 0.2- and 0.3-wt % agar are 2005 and 4210 s, respectively. It is suggested that the stress relaxation of 0.2-wt % agar gel by flow is faster than the 0.3-wt % agar gel. We can conclude that 0.2-wt % agar gel is a more viscous fluid than the 0.3-wt % agar gel. The relaxation curve may be given by $x = a - b \log_{10} t$, where x is load, t is time, and a and b are constants listed in Table II. This type of relaxation curve that was explained by the complicated spring-dashpot model (the Kelvin chain) was also reported in high polymer gels [36].

III. RESULTS

A. Three kinds of intrusion patterns

Figure 4 shows snapshots of dynamical interfacial growth

TABLE II. Parameters of the stress relaxation curve of agar gel.

Concentration of agar (%)	Deformation (mm)	a	b
0.2	3	1.62	0.47
0.2	2	0.74	0.22
0.3	3	3.38	0.96
0.3	2	3.14	0.94

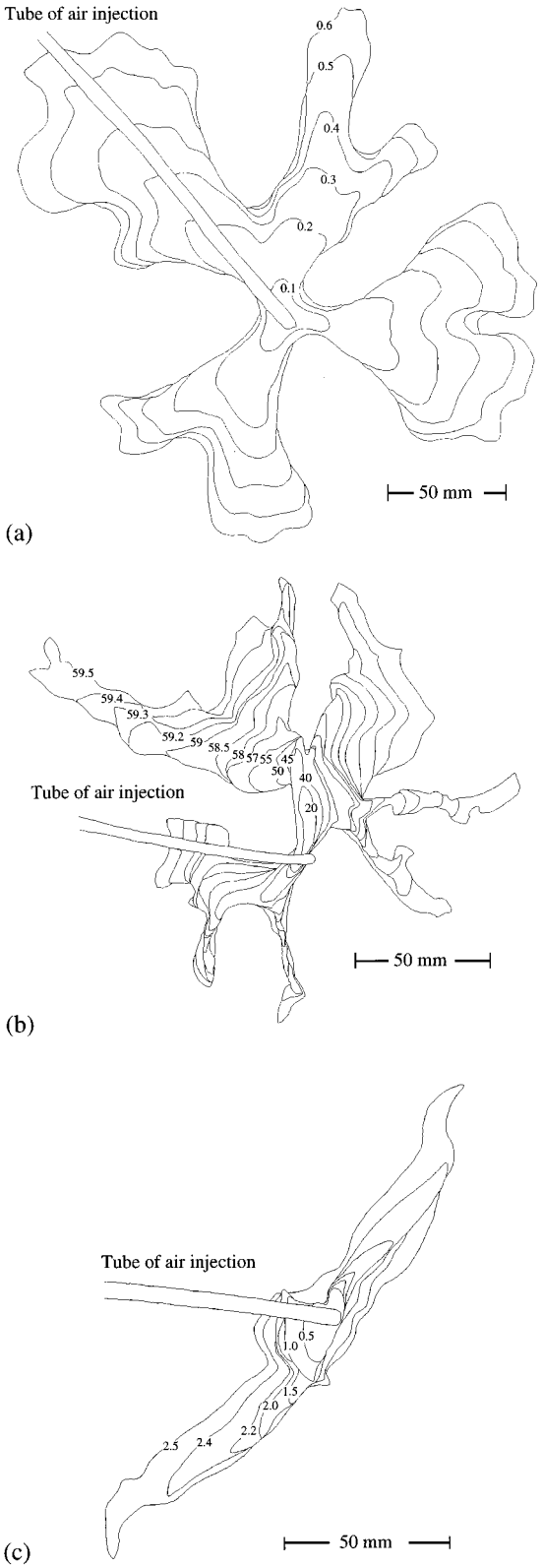

FIG. 4. Evolutions of the patterns observed by air injection into Hele-Shaw cell filled with agar gels: (a) The VF pattern is obtained in the agar gel with the concentration of 0.1-wt % agar and the injection pressure of air is 2.5 kPa. (b) The VEF pattern is obtained in the agar gel with a concentration of 0.2-wt % agar and the injection pressure of air is 2.0 kPa. (c) The SPC pattern obtained in the agar gel with a concentration of 0.3-wt % agar, and the injection pressure of air is 3.5 kPa. The number in the figure indicates the time measured from the start of air injection measured in seconds.

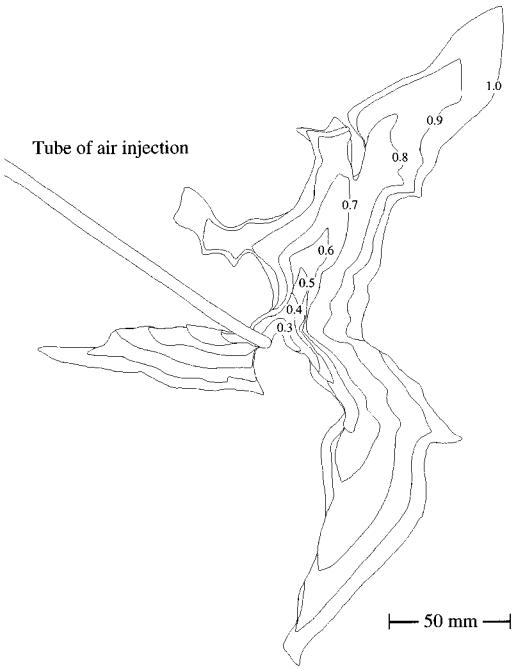

FIG. 5. Same as Fig. 3. Examples of the evolution of VEF patterns. The agar gel with the concentration of 0.2 wt % was used. The injection pressure of air is 3.5 kPa.

due to air intrusion into viscoelastic materials. The patterns can be classified into three kinds of patterns: a viscous fingering (VF) pattern [Fig. 4(a)], a viscoelastic fracturing (VEF) pattern [Fig. 4(b)], and a single plane cracking (SPC) pattern [Fig. 4(c)]. Under a constant injection pressure ranging from 0.5 to 4.5 kPa at every 0.5 kPa, the experiments of air injection into the Hele-Shaw cell filled with agar gels with concentrations of 0.1-, 0.2-, and 0.3-wt % agar were carried out systematically. In the case of the agar gel with a lower concentration of agar (0.1 wt %), the pattern obtained in our experiments resembles the VF patterns obtained in the water injection experiments of a Hele-Shaw cell filled with an aqueous clay slurries containing 10% by weight of bentonite [37] rather than the viscous fingering patterns obtained in the air injection experiments of a Hele-Shaw cell filled with glycerine [2]. Figure 4(a) shows an example of the viscous fingering pattern obtained in the agar gel with the concentration of 0.1-wt % agar. The VF patterns have two primary features: (1) a branched pattern and (2) the shape of growing tip is round.

On the other hand, in the case of the agar gels with higher concentration of agar (0.3 wt %), SPC patterns such as those observed in hydraulic fracturing or magma eruption are obtained. This is in contrast to the VF pattern obtained in the agar gels with lower concentration of agar. A SPC pattern

TABLE III. Characterization of three growth patterns.

Pattern	Branching	Tip geometry
SPC	No	Acute
VEF	Yes	Acute
VF	Yes	Round

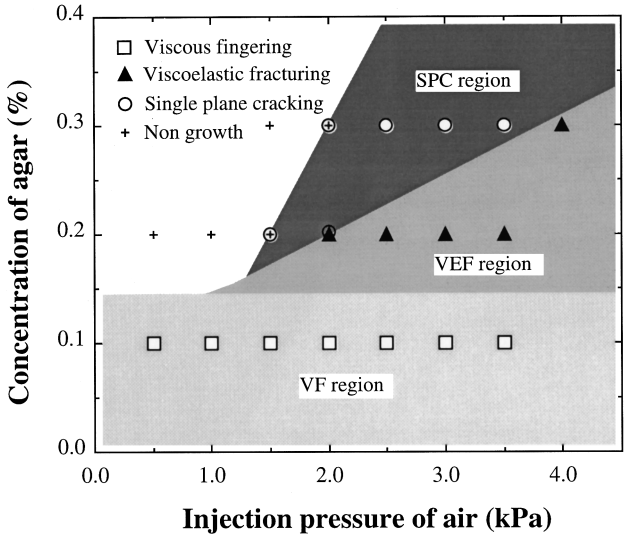

FIG. 6. Phase diagram for pattern formation by fluid injection. Both the pressure of air injection and the concentration of agar are experimental parameters.

due to fluid injection generates a penny shape crack in three-dimensional space, as observed in dikes in nature [17–19]. In two-dimensional space, it appears as a single line, i.e., a thin ellipse according to a linear elastic theory. The SPC pattern is generated by a tensile fracture. At first a small initial crack nucleates, and extends slowly and steadily, and then begins to grow rapidly at a certain size. Under a constant fluid injection pressure, the crack propagation is unstable [38]. The selective growth of crack at both ends occurs due to the stress concentration at the both ends of crack. Although a crack having a line geometry at the initial stage grows ideally like a single line, the initial geometry of the crack is strongly reflected in the SPC growth pattern: if the crack has three branches at the initial stage, the growth pattern having three branches structure appears, notwithstanding each branch grows like a line without branching. Therefore, such a growth pattern was categorized into SPC patterns in this study. In contrast to round tip in the VF pattern, the geometry of growth tips is acute due to tensile fracture in the SPC pattern.

The morphological feature of VEF patterns is summarized by two characteristics as follows: (1) a branched pattern, and (2) an acute growing tip. The acute growing tip results from tensile fracturing at the tip. Therefore, the acute growing tip of a VEF pattern suggests that the tips grow due to tensile fracturing in VEF pattern growth. Although there is a small variation in the morphology of classified VEF patterns as to whether they resemble rather SPC or VF patterns, the VEF patterns have the previously mentioned feature [see Figs. 4(b) and 5]. Two patterns classified as VEF patterns, as shown in Figs. 4(b) and 5, obtained in the agar gels with the same concentration of 0.2-wt % agar may give us different impressions in their appearance. One has a faint resemblance to the SPC pattern, and the other has a distant resemblance to the VF pattern. However, those patterns also have the features of VEF patterns: they are branched patterns and have acute growing tips. The VEF pattern is a quite different pattern from the VF and SPC patterns. The morphological differences among three patterns are summarized in Table III.

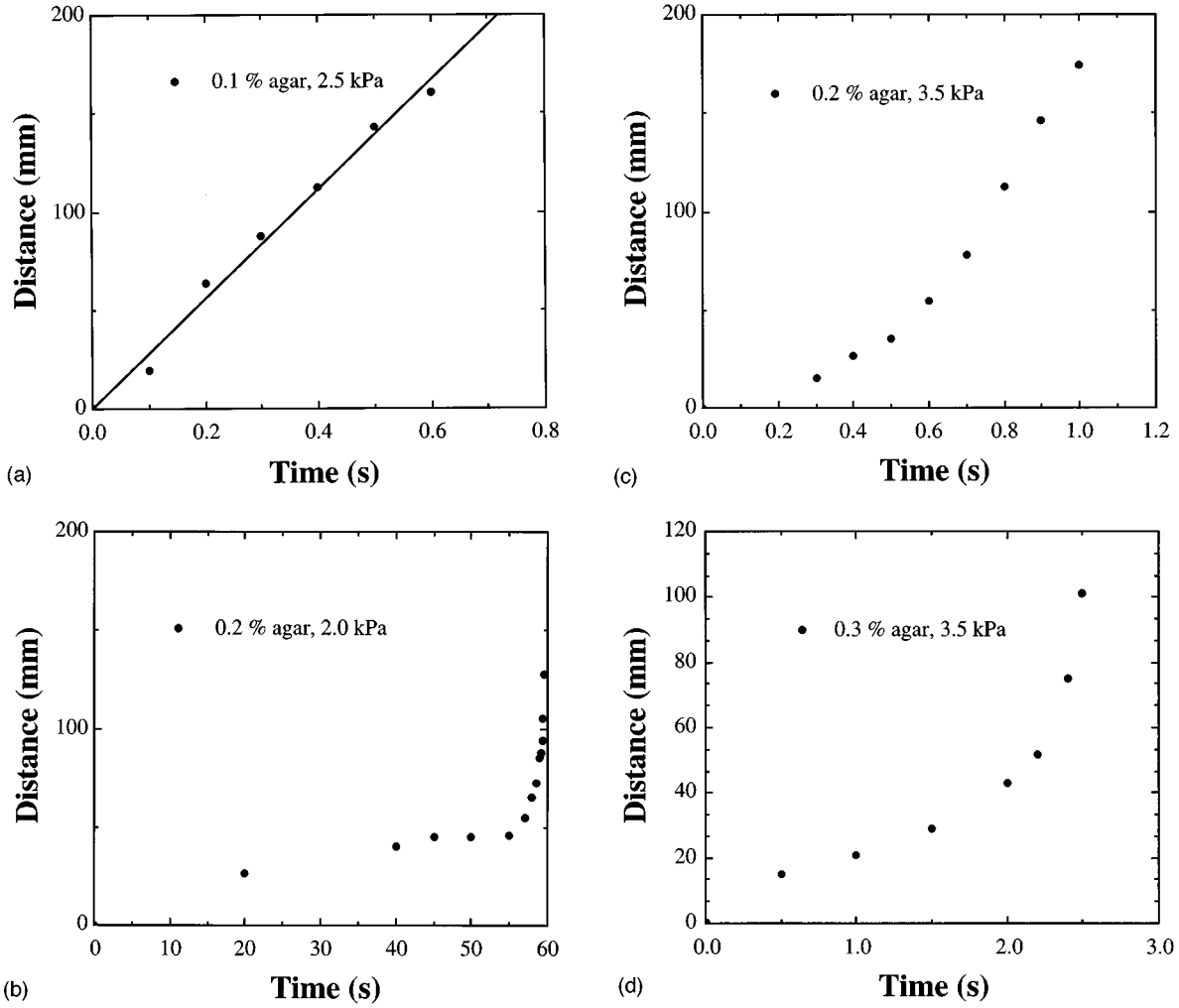

FIG. 7. The distance of the maximum branch measured from the center air injection hole is plotted against the time. (a) is the same as in Fig. 4(a), (b) as in Fig. 4(b), (c) as in Fig. 5, and (c) as in Fig. 4(c).

B. Phase diagram

How do three kinds of patterns appear as a function of experimental conditions? Figure 6 is a phase diagram based on the results of our experiments. Both the injection pressure of air and the concentration of agar are control parameters. Three types of agar gels with the concentration of agar, 0.1, 0.2, and 0.3 wt %, were used. An injection pressure of air was changed from 0.5 to 4.5 kPa every 0.5 kPa. The experiments at each experimental condition were repeated several times. Therefore, two different patterns overlap at the same experimental condition where there is a boundary of transition between patterns.

Let us consider the feature of this phase diagram. When the injection pressure is fixed, the pattern changes from the VF pattern to the SPC pattern via the VEF pattern with the increase of the concentration of agar. If the concentration of agar is kept fixed, the pattern changes from the SPC pattern to the VEF pattern with the increase of the injection pressure, except in the case of 0.1-wt % agar. In the case of the 0.1-wt % agar, only the VF pattern appeared at any injection pressure. Although 0.2- and 0.3-wt % agar show the properties of viscoelastic body, this result suggests that 0.1-wt % agar gel behaves essentially as a viscous fluid.

According to the stability analysis of the viscous fingering in a Hele-Shaw cell [7], the wavelength of the perturbation with the highest growth rate λ_m is given by

$$\lambda_m = \pi b \left(\frac{\sigma}{U\mu} \right)^{1/2}. \tag{3.1}$$

Here b is the distance of the two plates of the Hele-Shaw cell, σ is the interfacial tension between the two fluids, μ is the viscosity, and U is the flow velocity. Assuming that the interfacial tension between the air and the 0.1-wt % agar gel is the same value of the interfacial tension between the air and the pure water, the most unstable wavelength λ_m was estimated by using the moving interface velocity observed in Fig. 4(a). It is interesting to note that the wavelength of maximum instability $\lambda_m = 4.5$ cm is quite close to the observed wavelength of approximately 4.4 cm in Fig. 4(a).

The boundary between the SPC region and the nongrowth region can be explained by a tensile fracture. The tensile stress at the injection hole with circle geometry is equivalent to the injection pressure of air. The rough estimated value of the tensile strength of 0.3-wt % agar gel (1.7 kPa) coincides with the boundary value of 0.3-wt % agar gels. Once a crack

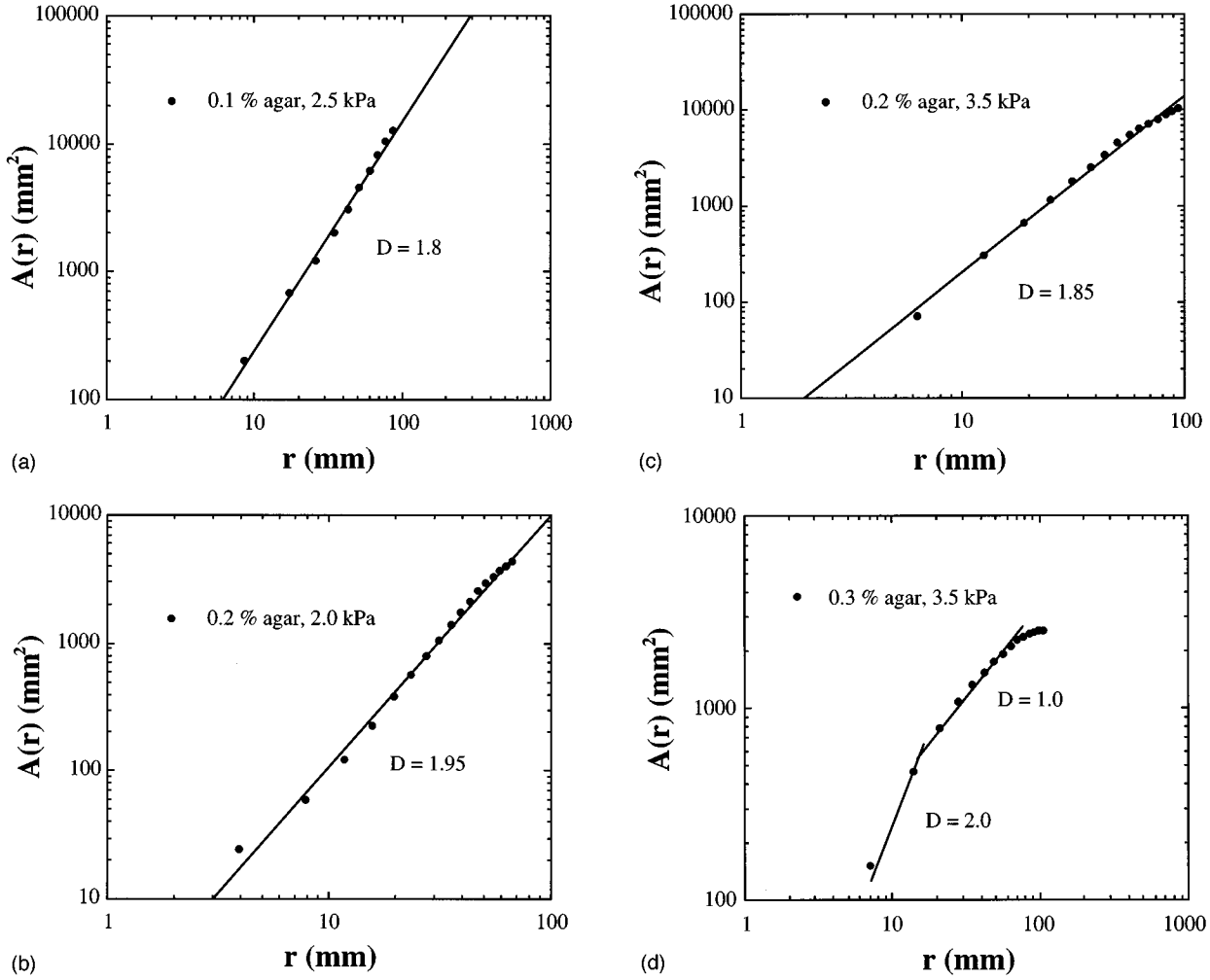

FIG. 8. The surface area covered by air within a circle of radius r, $A(r)$, is plotted against r. (a) is for the pattern at 0.6 s in Fig. 4(a), (b) is for the one at 59.5 s in Fig. 4(b), (c) is for the one at 1.0 s in Fig. 5, and (d) is for the one at 2.5 s in Fig. 4(c).

is generated, the tensile stress at the crack tip increases with the crack length l as a function of $\sqrt{l}$ according to a theory of linear elastic fracture mechanics.

The patterns appearing during air intrusion into viscoelastic materials result from the competition between viscous flow and fracturing. The length of the maximum branch is plotted against the time in Fig. 7. The abrupt pattern growth occurs at a certain size in the VEF pattern under our experimental condition of a constant air injection pressure. The crack propagation, i.e., the occurrence of fracture, depends on both the geometry of the crack and the strength of materials. The stress concentration occurs at the crack tips, which cause the tensile fracture. According to the theory of linear elastic fracture mechanics, this effect is explained in the term of the stress intensity factor as a function of crack geometry. The change of geometry of the crack owing to previous viscous flow causes the stress concentration at the growing tip, and bring about the tensile fracture.

The fractal dimensions of three intrusion patterns (Figs. 4 and 5) were calculated. The area covered by air within a circle of radius r, $A(r)$, was plotted against r in log-log plots shown in Fig. 8. Power laws were obtained for the VF and VEF patterns. The regression lines in Fig. 8 are determined by using the least-square method and the fractal dimensions were calculated from the slope of the regression lines. The fractal dimension D was 1.8 and 1.85–1.95 for the VF pattern (0.1-wt % agar), and the VEF pattern (0.2-wt % agar), respectively. This may be a preliminary result because of the small range of scaling law. For the SPC pattern, a log-log plot of $A(r)$ versus r does not follow a straight line. Since the geometry of the SPC is a line with a certain width, $A(r)$ increases as r^2 for small r and increases as r^1 for large r.

IV. DISCUSSION

Fractal geometry in fracture patterns may be a result of a Laplacian growth, which is realized, for example, in dielectric breakdown: this is a quasistatic pattern growth. The values of the fractal dimension for the VEF patterns are considerably different from the value $D=1.68$ for diffusion-limited aggregation (DLA) [14]. Fractal dimensions of 1.68, 1.76, and 1.84 were reported for the water–clay–water instability patterns of clay and water=0.06, 0.07, and 0.10 (w/w), respectively [37]. The mechanical properties of clay-water systems change from fluid suspensions to plastic pastes and finally to brittle solid with increasing the ratio of clay to water. The fractal dimension $D=1.68$, almost the same value for

DLA, was only obtained at the clay-water ratio of 0.06 (the mechanical properties of the clay-water system may be one of fluid suspensions.). At the range of mechanical properties of plastic pastes or brittle solids, the fractal dimensions for the water–clay-water instability patterns are higher and similar value obtained for the VEF pattern. Although many studies of quasi-static pattern growth by fracturing have been carried out recently [25,26,29,30], rather few studies concerned with dynamical pattern growths such as a crack propagation in brittle materials have been performed [31,39]. Dynamical crack propagation has a growth speed of an order of about 0.6 shear wave velocity in brittle material. The shear wave velocity of typical brittle materials such as glass, ceramics, and rocks is more than 1 km/s, which makes the measurement of the dynamical growth profile difficult. Since the elastic modulus of the shear stress of agar is very small, we can measure the dynamical growth due to crack propagation by using a video camera. The shear wave velocity is a function of the shear modulus. We can succeed in measuring an interfacial growth by air injection dynamically, as shown in Figs. 4 and 5, due to a small shear modulus of agar gels. However, an intrusion pattern by hydraulic fracturing (SPC) shows nonfractal geometry. In our experiment, the fractal geometry that appears in Laplacian growth [7,8] is not observed in both VEF and SPC patterns.

Previous experiments [32] were preformed at a constant injection flow rate. However, fluid intrusion into viscoelastic materials often occurs not under a constant intrusion flow rate but under a constant injection pressure of fluid in nature: e.g., magma intrusion [18,19]. Therefore, it is important to carry out an experiment of fluid injection into viscoelastic materials under a constant injection pressure. Our experiments were performed under a constant injection pressure of air. In our experimental condition, the growth of fracture is unstable according to a stability analysis of crack propagation [38].

There are some experiments concerning the pattern formation governed by the fluid flow between plates. The analog experiments that two glass slides held together by viscous medium (grease or fluid rubber cement) were slowly separated were demonstrated to simulate the formation of the so-called ''river pattern'' seen at microscopic fracture surfaces [40,41]. Although at a first glance the pattern of the medium (grease) observed in the analog experiment [40] seems to resemble the VEF patterns of the intruding fluid, it should note that the intruding fluid patterns do not resemble the VEF patterns. The formation of the patterns obtained by their experiments is a result of Taylor instability (viscous fingering) [42].

A new kind of pattern growth, viscoelastic fracturing, was observed by means of fluid injection into Hele-Shaw cell filled with viscoelastic materials. In our experiment, two typical interfacial growth patterns observed in a viscous fluid and a brittle solid, namely, the VF and SPC patterns, were also observed in our viscoelastic materials of the agar gel along with the VEF pattern. Those patterns are formed due to quite different stress release mechanisms; the former is a result of viscous flow, and the latter is a result of fracture. There are few studies of seamless observation from single crack fracturing to a viscous finger due to fluid injection, which give us total understanding of fluid intrusion phenomena. Viscoelastic materials are classified into two categories according to stress relaxation behavior at a long time limit; a fluid (e.g., a Maxwell fluid) or a solid (e.g., a Kelvin solid). Previous studies of a fluid injection into a viscoelastic material (clay-water system) were carried out in a viscoelastic fluid. In our experiments, the viscoelastic solid is used as a viscoelastic material. We focused on the fracture in comparison with the previous studies. This success of the reproduction of the transition from the SPC pattern to the VF pattern via the VEF pattern by carrying out systematic experiments is the first step of understanding of interfacial growth in viscoelastic materials, which give us a total understanding of brittle fracturing and viscous flow.

ACKNOWLEDGMENTS

I would like to thank S. Torquato, M. D. Rintoul, H. Cheng, and T. Ogawa for useful discussions. This research was supported by the Grant-in-Aid for Research from the Ministry of Education (No. 0484023) and the Gakunai Project of the University of Tsukuba.

[1] M. D. Savage, J. Fluid Mech. **80**, 743 (1977); **80**, 757 (1977).
[2] L. Paterson, J. Fluid Mech. **113**, 513 (1981).
[3] P. G. Saffman, J. Fluid Mech. **173**, 73 (1986).
[4] D. Bensimon, L. P. Kadanoff, S. Liang, B. I. Shraiman, and C. Tang, Rev. Mod. Phys. **58**, 977 (1986).
[5] J. Nittmann, G. Daccord, and H. E. Stanley, Nature (London) **314**, 141 (1985).
[6] G. Daccord, J. Nittmann, and H. E. Stanley, Phys. Rev. Lett. **56**, 336 (1986).
[7] J. Feder, *Fractals* (Plenum, New York, 1988).
[8] T. Vicsek, *Fractal Growth Phenomena* (World Scientific, Singapore, 1989).
[9] L. Paterson, Phys. Rev. Lett. **52**, 1621 (1984).
[10] L. Niemeyer, L. Peitronero, and H. J. Wiesmann, Phys. Rev. Lett. **52**, 1033 (1984).
[11] J. S. Langer, Rev. Mod. Phys. **52**, 1 (1980); Science **243**, 1150 (1989).
[12] J. Nittmann and H. E. Stanley, Nature (London) **321**, 663 (1986).
[13] D. A. Kessler, J. Koplik, and H. Levine, Adv. Phys. **37**, 255 (1988).
[14] T. A. Witten and L. M. Sander, Phys. Rev. Lett. **47**, 1400 (1981); Phys. Rev. B **27**, 5686 (1983).
[15] R. M. Brady and R. C. Ball, Nature (London) **309**, 225 (1984).
[16] M. Matsushita, M. Sano, Y. Hayakawa, H. Honjo, and Y. Sawada, Phys. Rev. Lett. **53**, 286 (1984).
[17] J. Green and M. Short, *Volcanic Landforms and Surface Features—A Photographic Atlas and Glossary* (Springer-Verlag, Berlin, 1971).
[18] G. Baer and A. Heimann, *Physics and Chemistry of Dykes:*

Selected Papers Presented at the Third International Dyke Conference Jerusalem, Israel, 4–8 September 1995 (Balkema, Rotterdam, 1995).
[19] A. M. Rubin, Annu. Rev. Earth Planet Sci. **23**, 287 (1995).
[20] *Hydraulic Fracturing Stress Measurements*, edited by B. C. Haimson, special issue of Int. J. Rock Mech. Min. Sci. Geomech. Abstr. **26**, pp. 445–685 (1989).
[21] F. H. Harlow and W. E. Pracht, J. Geophys. Res. **77**, 7038 (1972).
[22] J. Haraden, Energy **17**, 777 (1992).
[23] F. Tzschichholz, H. J. Herrmann, H. E. Roman, and M. Pfuff, Phys. Rev. B **49**, 7056 (1994).
[24] F. Tzschichholz and H. J. Herrmann, Phys. Rev. E **51**, 1961 (1995).
[25] E. Louis and F. Guinea, Europhys. Lett. **3**, 871 (1987).
[26] P. Meakin, G. Li, L. M. Sander, E. Louis, and F. Guinea, J. Phys. A **22**, 1393 (1989).
[27] H. J. Herrmann and S. Roux, *Statistical Models for the Fracture of Disordered Media* (North-Holland, Amsterdam, 1990).
[28] J. Fineberg, S. P. Gross, M. Marder, and H. L. Swinney, Phys. Rev. Lett. **67**, 457 (1991).
[29] M. Sahimi, Physica A **186**, 160 (1992).
[30] H. Colina, L. de Arcangelis, and S. Roux, Phys. Rev. B **48**, 3666 (1993).
[31] F. F. Abraham, D. Brodbeck, R. A. Rafey, and W. E. Rudge, Phys. Rev. Lett. **73**, 272 (1994).
[32] E. Lemaire, P. Levitz, G. Daccord, and H. Van Damme, Phys. Rev. Lett. **67**, 2009 (1991).
[33] Wilhelm Flügge, *Viscoelasticity* (Springer-Verlag, Berlin, 1975).
[34] T. Matsuhashi, in *Food Gels*, edited by P. Harris (Elsevier, London, 1990).
[35] R. Lapasin and S. Pricl, *Rheology of Industrial Polysaccharides: Theory and Applications* (Blackie, London, 1995).
[36] K. Ogino, Y. Osada, T. Fushimi, and A. Ymauchi, Gel (Sangyo-tosho, Tokyo, 1991).
[37] Henri Van Damme, Francois Obrecht, Pierre Levitz, L. Gatineau, and Claude Laroche, Nature (London) **320**, 731 (1986).
[38] H. J. Herrmann and J. Kertész, Physica A **178**, 227 (1991).
[39] M. Marder and Xiangming Liu, Phys. Rev. Lett. **71**, 2417 (1993).
[40] C. A. Pampillo and A. C. Reimschuessel, J. Mater. Sci. **9**, 718 (1974).
[41] F. Spaepen and D. Turnbull, Scr. Metall. **8**, 563 (1974).
[42] F. Spaepen, Acta Metall. **23**, 615 (1975); R. J. Fields and M. F. Ashby, Philos. Mag. **33**, 33 (1976).